Original Article | Open Access

Artificial Intelligence Surgery

Li *et al. Art Int Surg.* 2026;6:579-97 **DOI:**10.20517/ais.2026.88

Robotic navigation and precision in lung nodule microwave ablation

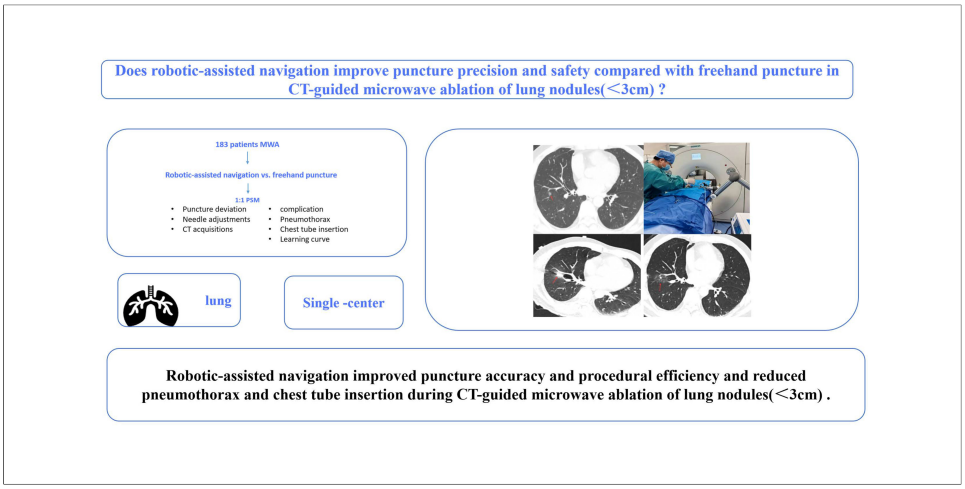
Lilong Li[1,#], Li Qiu[1,#], Hanghui Liu[2,#], Lisheng Huang[1], Fei Cui[1], Xuekun Zhang[1], Yunlong Qu[1], Hengrui Liang[1], Jun Liu[1], Xingyang Xue[1]

Keywords:
Robotic-assisted navigation, microwave ablation, propensity score matching, lung nodule

Citation: Li L, Qiu L, Liu H, Huang L, Cui F, Zhang X, Qu Y, Liang H, Liu J, Xue X. Robotic navigation and precision in lung nodule microwave ablation. *Art Int Surg.* 2026;6:579-97. https://dx.doi.org/10.20517/ais.2026.88

Received: 25 Aug 2026 **First Decision:** 30 Sep 2026 **Revised:** 18 Oct 2026 **Accepted:** 21 Oct 2026 **Published:** 27 Oct 2026

Academic Editor: Andrew Gumbs **Copy Editor:** Tong Wang **Production Editor:** Tong Wang



Abstract

Aim: Robotic-assisted puncture systems have been developed, but evidence for their use in percutaneous microwave ablation (MWA) of lung nodules remains limited.

Methods: This retrospective single-center study included 183 patients who underwent computed tomography (CT)-guided percutaneous MWA for pulmonary nodules < 3 cm between March 2024 and April 2025. Patients underwent robotic-assisted or conventional freehand puncture. After 1:1 propensity score matching, technical success, puncture deviation, intraprocedural CT acquisitions, needle adjustments, and complications were compared. Multivariable logistic regression, subgroup analyses, and learning-curve analysis were performed. The study was approved by the Institutional Review Board of the First Affiliated Hospital of Guangzhou Medical University (ES-2026-K212-02) on 23 June 2026. The requirement for individual written informed consent for study participation was waived due to the retrospective nature of the study; patients were covered under the hospital's general informed consent for hospitalization. Written informed consent was obtained from all patients for the procedure.

[1]Department of Thoracic Surgery and Oncology, the First Affiliated Hospital of Guangzhou Medical University, State Key Laboratory of Respiratory Disease & National Clinical Research Center for Respiratory Disease, Guangzhou 510120, Guangdong, China.
[2]Department of Thoracic Surgery, Huizhou First Hospital, Huizhou 516001, Guangdong, China.
[#]These authors contributed equally to this work and share first authorship.

Correspondence to: Prof. Xingyang Xue, Prof. Jun Liu, Dr. Hengrui Liang, Department of Thoracic Surgery and Oncology, the First Affiliated Hospital of Guangzhou Medical University, State Key Laboratory of Respiratory Disease & National Clinical Research Center for Respiratory Disease, Guangzhou 510120, Guangdong, China. E-mail: xxy1023970@126.com; ljxwkgy@126.com; hengrui_liang@163.com

Results: After matching, 86 patients were included (43 per group), with comparable baseline characteristics and 100% technical success in both groups. Compared with freehand puncture, robotic-assisted navigation was associated with significantly reduced puncture deviation (median [IQR], 3.0 [2.0-4.5] *vs.* 6.0 [5.0-9.5] mm), intraprocedural CT scans (2.0 [1.5-2.0] *vs.* 5.0 [5.0-7.0]), and needle adjustments (2.0 [1.5-2.0] *vs.* 4.0 [3.0-4.0]; all $P < 0.01$). Robotic-assisted navigation was associated with a lower overall complication rate (46.51% *vs.* 81.40%; $P < 0.01$), driven mainly by reduced pneumothorax (27.91% *vs.* 69.77%; $P < 0.01$) and chest drain insertion rates (4.65% *vs.* 20.93%; $P = 0.02$). Multivariable analysis robotic-assisted puncture remained independently associated with a lower risk of pneumothorax (OR 0.160, 95%CI: 0.061-0.420, $P < 0.001$). Subgroup analyses showed consistent benefits across strata. Procedural performance stabilized after approximately 24 robotic-assisted cases.

Conclusion: Robotic-assisted navigation was associated with greater procedural precision, efficiency, and safety in CT-guided percutaneous MWA, while demonstrating consistent performance across different lesion characteristics and a relatively short learning curve. It may serve as a reproducible and standardized platform for percutaneous pulmonary ablation.

INTRODUCTION

Lung cancer remains one of the most frequently diagnosed malignancies and the leading cause of cancer-related mortality worldwide[1]. The widespread implementation of computed tomography (CT) screening has led to increasing detection of small pulmonary nodules, including early-stage primary lung cancers, suspected malignant nodules, and oligometastatic lung lesions, at potentially curable stages[2]. Although surgical resection remains the standard treatment for operable early-stage lung cancer and selected pulmonary metastases, many patients are not suitable candidates because of limited cardiopulmonary reserve, advanced age, comorbidities, prior treatment, technically challenging lesion locations, or personal preference. Consequently, image-guided percutaneous thermal ablation has emerged as an important minimally invasive local treatment option for lung nodules[3,4].

Among available ablation modalities, microwave ablation (MWA) has been increasingly adopted for the treatment of primary and metastatic lung tumors[5,6]. By generating electromagnetic energy-induced coagulative necrosis, MWA enables rapid tissue heating and the formation of a predictable ablation zone[7]. For small lung nodules, complete tumor coverage with an adequate safety margin is essential for technical success and durable local control[8,9]. Accurate antenna placement is therefore fundamental to treatment efficacy. Unlike diagnostic biopsy or preoperative localization procedures, therapeutic ablation requires precise antenna positioning to ensure complete lesion coverage while minimizing injury to surrounding lung parenchyma and adjacent structures[10,11].

Conventional CT-guided percutaneous MWA is typically performed using a freehand technique, whereby operators estimate the puncture entry site, trajectory, and insertion depth from two-dimensional CT images, followed by intermittent CT verification and manual needle adjustment[12]. Despite its widespread use, this approach remains highly operator-dependent and can be technically challenging, particularly for small or deeply located nodules, lesions adjacent to ribs or critical structures, and lower-lobe lesions affected by respiratory motion. Repeated needle manipulations may prolong procedural time, increase CT acquisition frequency and radiation exposure, and exacerbate parenchymal injury, thereby increasing the risk of complications such as pneumothorax and pulmonary hemorrhage[13,14]. Robotic-assisted navigation systems have therefore been developed to improve the precision and standardization of CT-guided percutaneous procedures by integrating three-dimensional reconstruction, trajectory planning, respiratory motion monitoring, and robotic arm-assisted needle guidance[15-18]. By translating CT-derived anatomical

information into a predefined physical puncture trajectory, these systems facilitate accurate needle placement and may enhance procedural efficiency while reducing operator dependence. Together, these robotic navigation platforms represent the physical execution layer of an emerging cognitive-physical loop for intelligent surgery, wherein patient-specific image-based planning and simulation are coupled with real-time, robot-assisted physical action[19].

Clinical evidence supporting robotic-assisted lung interventions is accumulating. In preoperative lung nodule localization, robotic-assisted navigation has been associated with higher first-pass success, improved localization accuracy, fewer CT acquisitions, and lower radiation exposure without increasing complication rates[20]. Robotic guidance has also shown feasibility and favorable targeting accuracy in CT-guided radiofrequency ablation and cryoablation of pulmonary metastases, particularly in technically challenging procedures requiring accurate probe positioning or multiple-probe deployment[21-23]. However, evidence from localization procedures cannot be directly extrapolated to MWA, as localization needles and ablation antennas differ substantially in diameter, rigidity, targeting requirements, and procedural objectives. Furthermore, previous studies have primarily evaluated robotic guidance in radiofrequency ablation or cryoablation, leaving its role in CT-guided percutaneous MWA of lung nodules insufficiently characterized. To address this gap, we conducted a retrospective propensity score-matched study comparing robotic-assisted navigation with conventional freehand CT-guided puncture during MWA of lung nodules. We assessed procedural performance, including technical success, puncture deviation, CT acquisition frequency, needle adjustments, complications, and the learning curve. We hypothesized that robotic-assisted navigation would maintain technical success while improving puncture accuracy and procedural efficiency, with the potential to reduce puncture-related complications.

METHODS

Study design and patients

This retrospective single-center cohort study was conducted in the Second Ward of Thoracic Surgery at The First Affiliated Hospital of Guangzhou Medical University. Consecutive patients who underwent pulmonary lesion ablation between March 2024 and April 2025 were screened. The inclusion criteria were as follows: (1) age ≥ 18 years; (2) maximum pulmonary lesion diameter < 3 cm; and (3) eligibility for pulmonary nodule ablation confirmed by a multidisciplinary team comprising thoracic surgeons, pulmonologists, and radiologists. Patients were excluded if they had (1) uncorrectable coagulation disorders; (2) an initial ablation modality other than MWA, such as cryoablation or radiofrequency ablation; or (3) severe cachexia or cardiopulmonary insufficiency, including severe pulmonary arterial hypertension. Of 227 screened patients, 183 met the eligibility criteria and were assigned to either the robotic-assisted navigation group (robotic group, n = 130) or the conventional freehand CT-guided group (freehand group, n = 53) [Figure 1].

Robotic-assisted optical navigation system

The robotic-assisted optical navigation platform used in this study was the TH-S1 system (TrueHealth Medical Technology Co., Ltd., Hengqin, China), a Class III medical device approved by the National Medical Products Administration of China. The system comprises three integrated modules: a robotic arm positioning and puncture unit, a surgical planning workstation, and an optical navigation system [Figure 2].

CT-guided percutaneous MWA procedure

Preoperative preparation

All procedures were performed in a CT-guided interventional suite equipped with a 64-detector scanner (SOMATOM Perspective, Siemens Healthineers). Patients underwent local infiltration anesthesia with 2% lidocaine, and vital signs were continuously monitored throughout the procedure. To minimize

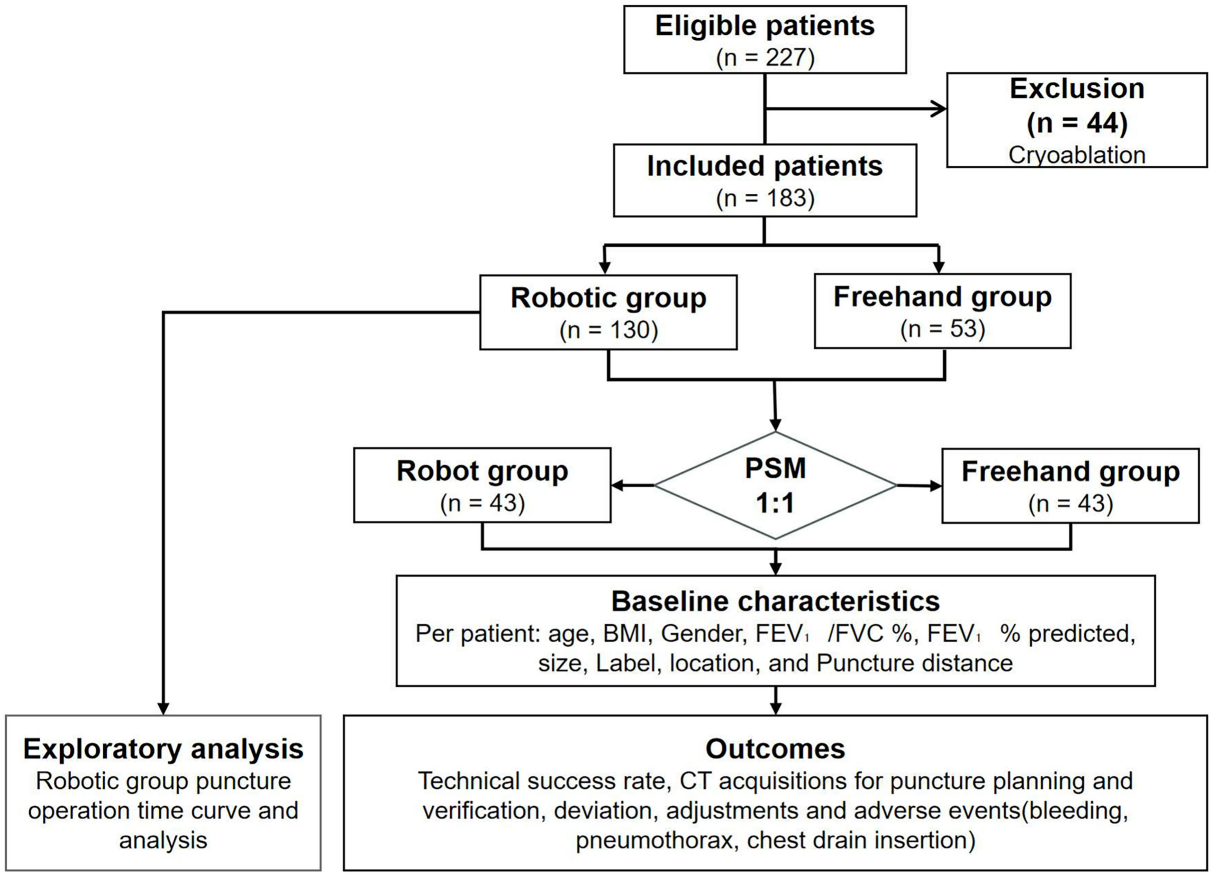


Figure 1. Flowchart of the study participants. Of 227 patients screened for eligibility, 44 were excluded because the initial ablation modality was cryoablation rather than MWA, leaving 183 eligible patients (130 robotic-assisted, 53 freehand). After 1:1 PSM with a caliper width of 0.1, 43 patients remained in each group (total *n* = 86). The matched cohort was used for primary comparative analysis, including multivariable logistic regression. Exploratory subgroup analyses were performed in the full pre-matching cohort (*n* = 183), comparing puncture deviation and needle adjustments across subgroups defined by lesion diameter, puncture distance, and lesion location. PSM: Propensity score matching; BMI: body mass index; FEV_1: forced expiratory volume in one second; FVC: forced vital capacity; CT: computed tomography; MWA: microwave ablation.

operator-related variability, all puncture procedures in both the robotic and freehand groups were performed by the same thoracic surgeon.

Robotic group

Thin-slice chest CT images (1-mm slice thickness and interval) were acquired and imported into the TH-S1 system for three-dimensional reconstruction of the target nodule, pulmonary vessels, bronchi, osseous structures, and skin surface. The optical navigation unit was used to automatically register patient positioning data to the reconstruction model, with registration error maintained within ±1 mm.

The system was used to plan the skin entry point, needle trajectory, and insertion depth. The robotic arm aligned the needle along the planned trajectory, and the operator then advanced it manually. Patients were instructed to maintain a reproducible end-expiratory breath-hold during CT acquisition and needle advancement. Respiratory stability was monitored using the respiratory-monitoring/gating function integrated into the robotic system. When breathing was unstable, CT acquisition and needle advancement were paused until a stable respiratory phase was restored. No separate external real-time respiratory-tracking system was used. Conventional step-and-shoot sequential CT was intermittently performed to verify needle

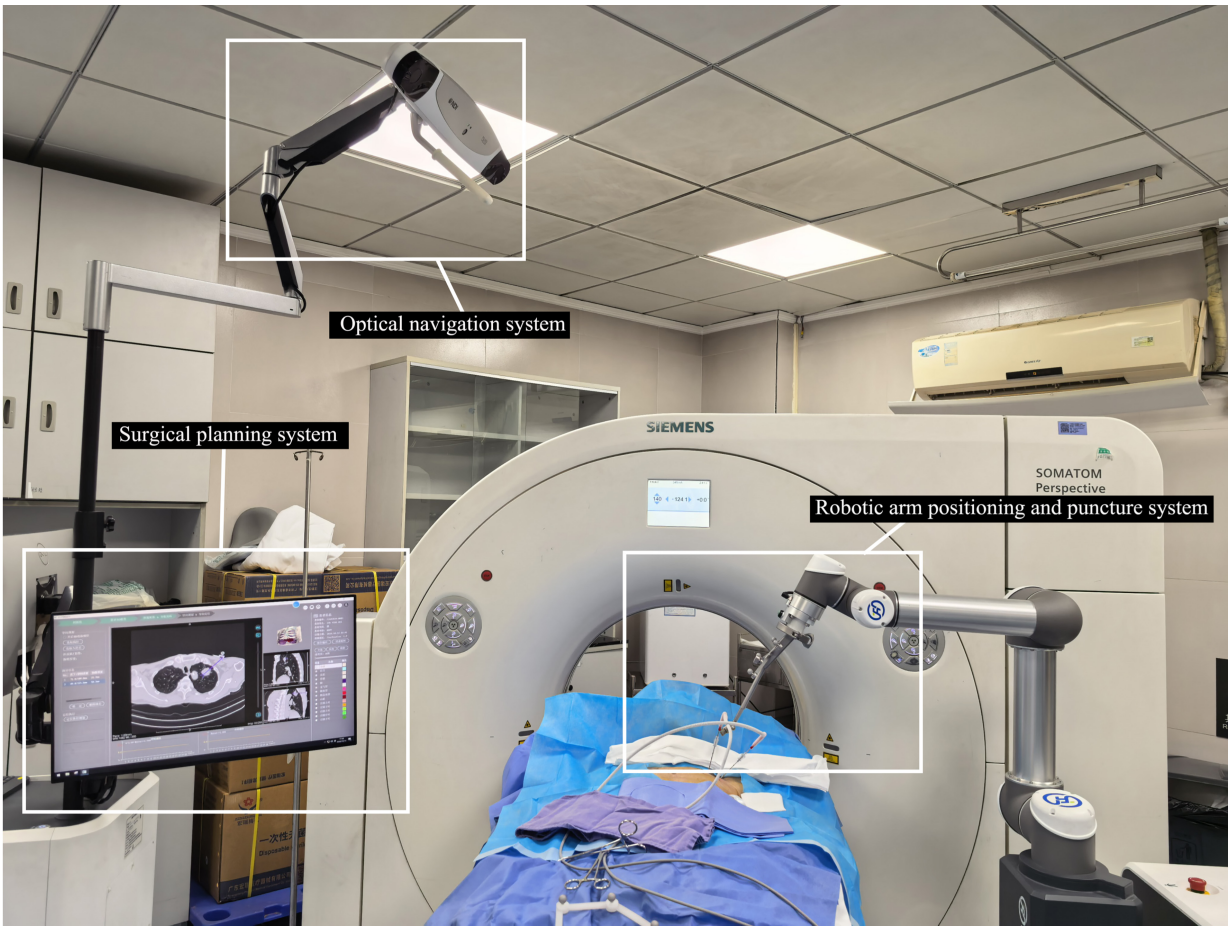


Figure 2. Robotic-assisted optical navigation system. It consists of three core components: a robotic arm positioning and puncture system, a surgical planning system, and an optical navigation system. The figure is an original photograph taken by the authors.

position and confirm the final needle-tip location. Manual trajectory correction was performed when necessary. After satisfactory needle placement was confirmed, MWA was performed using a KY-2000A system at 35-50 W. Two to three ablation cycles were delivered, with a total ablation time of 4-9 min [Figure 3].

Freehand group

In the freehand group, needle planning and placement were performed using conventional step-and-shoot sequential CT guidance and the scanner laser-guidance system. Patients were instructed to maintain a reproducible end-expiratory breath-hold during CT acquisition and needle advancement. Repeated sequential CT acquisitions were obtained to verify needle position, and manual trajectory corrections were performed when necessary. MWA was performed using the same protocol as that used in the robotic-assisted group.

Outcome measures

Endpoints included technical outcomes, safety outcomes, and exploratory learning-curve outcomes.

Technical outcomes comprised technical success, CT acquisition frequency, puncture deviation, and the number of needle adjustments. Technical success was assessed on immediate post-ablation CT and defined as complete lesion coverage with an ablation margin of at least 5 mm. Puncture deviation was defined as the Euclidean distance between the actual needle tip and the planned target, consistent with previous studies[24,25].

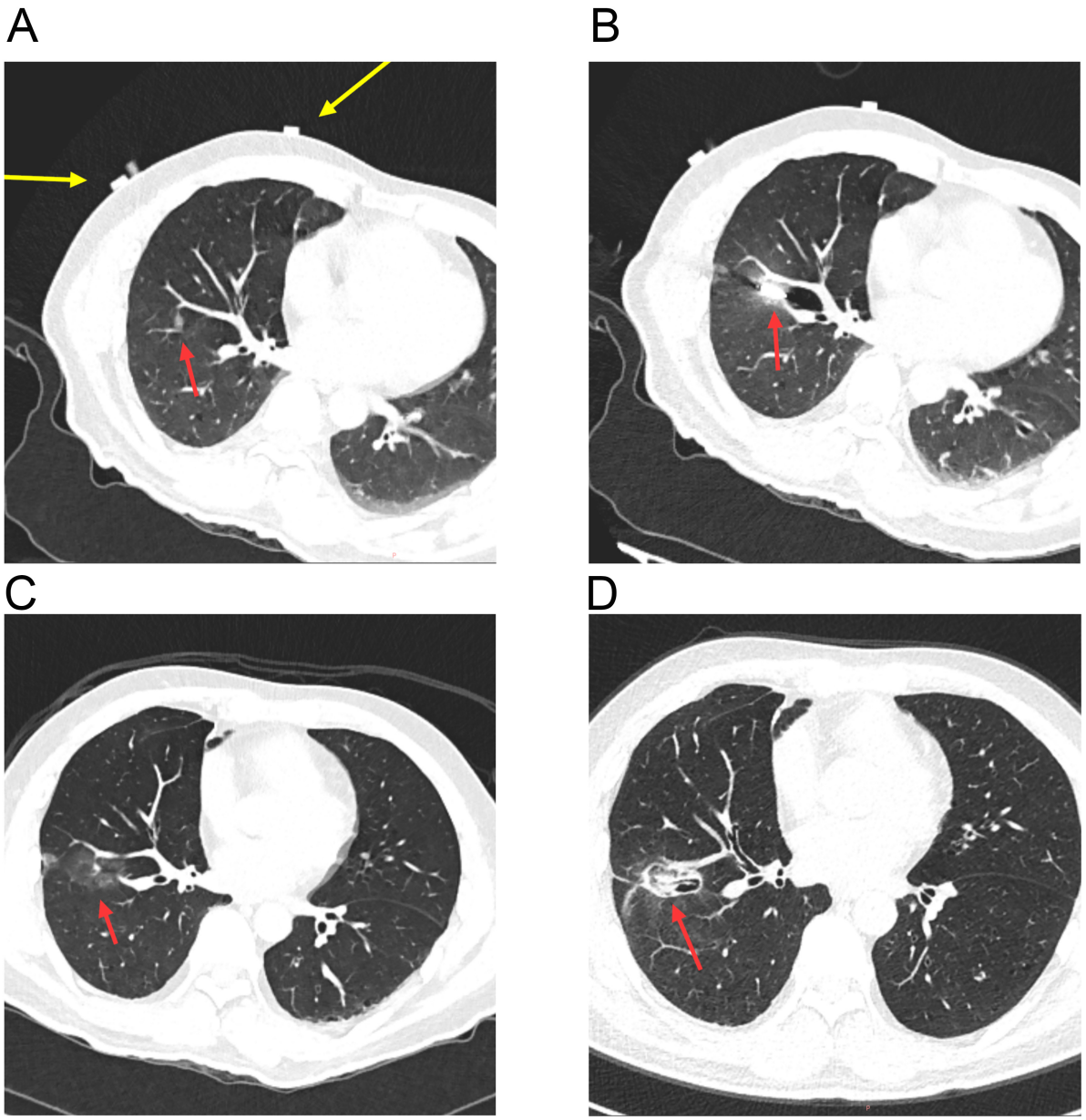


Figure 3. A robotic-assisted navigation system-guided MWA case. (A) The nodule is located in the right lower lobe. The yellow arrow indicates the CT visualization of the body surface positioning belt of the robotic-assisted navigation system, and the red arrow indicates the target nodule; (B) The puncture needle reaches the target in one pass, and MWA is initiated; (C) Immediate postoperative CT scan shows a clear ablation zone, with no pneumothorax or hemorrhage observed; (D) One-month follow-up CT after ablation reveals shrinkage and fibrosis of the ablation zone. MWA: Microwave ablation; CT: computed tomography.

A needle adjustment was defined as any deliberate correction of the needle trajectory after an interim CT scan showed that the needle tip or course deviated from the planned trajectory. Each correction cycle, consisting of partial or complete withdrawal followed by redirection and re-advancement, was counted as one adjustment.

The number of CT acquisitions was defined as the number of intermittent CT series performed from the beginning of puncture positioning to confirmation of the final needle-tip position, including the initial positioning/planning scan and all verification scans during needle advancement. CT scans obtained after completion of ablation were not included in this count. The same counting standard was applied to both the robotic-assisted and freehand groups.

In the freehand group, a target point corresponding to the intended final needle-tip position was selected by the operator on the planning CT before puncture, chosen to ensure an ablation margin of at least 5 mm, and recorded in the planning images in the same way as the system-defined target in the robotic group. After the procedure, the actual needle-tip position was identified on the final verification CT using multiplanar reconstruction, and the three-dimensional Euclidean distance between the actual tip and the pre-specified target was calculated using the built-in measurement tool of the CT workstation[20]. The identical measurement method was used in both groups.

Safety outcomes included procedure-related hemorrhage, pneumothorax, chest drain insertion, and other adverse events occurring during the procedure or within 1 day thereafter.

The overall complication rate was defined as the proportion of patients experiencing at least one complication during this period, with each patient counted only once regardless of the type or number of complications. Thus, a patient who developed both pneumothorax and hemorrhage was counted as one patient with complications in the overall analysis.

Pneumothorax was defined as any newly developed pleural air collection detected on imaging during the procedure or within 1 day thereafter. All imaging-detected pneumothoraces were recorded, regardless of symptoms or the need for intervention. Intervention-requiring pneumothorax was defined as pneumothorax associated with dyspnea, chest tightness, or other respiratory discomfort and requiring chest tube drainage. The decision to place a chest tube was based on the patient's symptoms, clinical condition, and imaging findings.

Procedure-related hemorrhage included new or increased pulmonary parenchymal hemorrhage, hemothorax, hemoptysis, or other hemorrhage attributable to the procedure. Hemorrhage severity was graded according to the Society of Interventional Radiology (SIR) adverse-event classification system[26]. Only Grade A and B hemorrhagic events occurred in this study; no Grade C or higher events were observed.

Propensity score matching (PSM)

Patients were not randomly assigned to robotic-assisted or freehand treatment. After initial evaluation, the treating physician assessed the technical feasibility of both approaches based on lesion characteristics (including size, location, and depth from the pleural surface) and discussed the respective procedures, potential benefits, and risks of each option with the patient. The final treatment decision was made by the patient based on personal preference after receiving this information. In cases where one approach was deemed technically infeasible based on lesion characteristics, patients were counseled accordingly. To reduce potential selection bias and improve comparability between the robotic-assisted and freehand groups, propensity scores were estimated using a multivariable logistic regression model, with treatment group as the dependent variable. Puncture distance was not included in the propensity score model because it is an intraprocedural variable that is not available at the time of treatment assignment and therefore cannot serve as a pre-treatment covariate for matching; it was instead included in the post-matching multivariable regression model to adjust for its potential confounding effect. The prespecified covariates were age, sex, body mass index (BMI), forced expiratory volume in one second (FEV_1)% predicted, lesion diameter, pulmonary lobe, and lesion location. Continuous variables were entered as continuous terms, and categorical variables were entered as indicator variables. Patients were matched at a 1:1 ratio using nearest-neighbor matching without replacement. The caliper width was set at 0.1 on the absolute propensity-score scale, meaning that the absolute difference in propensity scores between matched patients could not exceed 0.1.

After matching, 43 patients remained in each group. The overlap of propensity-score distributions was assessed before and after matching using density plots and the observed propensity-score ranges. Covariate balance was evaluated using standardized mean differences (SMDs), with an absolute SMD below 0.10 considered indicative of adequate balance and an SMD of 0.10 to 0.20 considered indicative of small residual differences. No missing data were observed for any covariates included in the propensity-score model; therefore, no imputation was performed.

All imaging-based outcomes, including pneumothorax, hemorrhage, puncture deviation, and technical success, were independently assessed by a radiologic technologist who was not involved in the procedure.

Multivariable analysis and subgroup analyses

Separately from the PSM model used for cohort matching (which included age, sex, BMI, FEV_1% predicted, lesion diameter, pulmonary lobe, and lesion location), a post-matching multivariable logistic regression model was fitted in the propensity score-matched cohort to identify factors independently associated with pneumothorax. Covariates were selected a priori according to clinical relevance and potential confounding effects. The final model included puncture method, age, BMI, lesion diameter, pulmonary lobe, and puncture distance. Adjusted odds ratios with 95% confidence intervals were reported. Pulmonary lobe was coded as a binary variable (upper lobe *vs.* middle/lower lobe) based on clinical relevance. The matched cohort included 42 pneumothorax events, yielding an events-per-variable ratio of 7:1 for the 6-covariate model.

Exploratory subgroup analyses were performed in the full pre-matching cohort (n = 183), in which puncture deviation and needle-adjustment frequency were compared between groups across strata defined by puncture distance, pulmonary lobe, and lesion diameter. Effect modification was assessed using linear regression models containing the treatment, subgroup covariate, and treatment-by-covariate interaction terms; puncture deviation was log-transformed to address skewness. The interaction tests were repeated in the propensity score-matched cohort as a sensitivity analysis. Additional analyses within the robotic-assisted cohort assessed whether lesion characteristics influenced puncture performance.

Learning-curve analysis

All 130 consecutive robotic-assisted procedures were performed by a single experienced thoracic surgeon with extensive prior experience in freehand CT-guided puncture but no prior experience with robotic-assisted navigation. The procedures were analyzed chronologically to assess the effect of operator experience with the robotic system. A one-phase exponential decay model was fitted using procedure number as the independent variable and the interval from first CT acquisition to successful needle placement as the dependent variable. The 50%, 75%, and 90% learning milestones were defined as the case numbers corresponding to the respective reductions from the initial value to the plateau. Based on the curve plateau, procedures were divided into learning and proficient phases, and procedural metrics and complication rates were compared between phases.

Statistical analysis

All analyses were performed using Python. Demographic and physiological variables (age, BMI, and FEV_1% predicted) were presented as mean ± standard deviation (SD) in accordance with standard clinical reporting conventions. For all other continuous variables, normality was assessed using the Shapiro-Wilk test; normally distributed variables were presented as mean ± SD, and non-normally distributed variables were presented as medians with interquartile ranges (IQR). Between-group comparisons for continuous variables were performed using the independent-samples t test (Welch's t test when variances were unequal) for mean ± SD variables and the Mann-Whitney U test for median [IQR] variables. Categorical variables were presented as frequencies with percentages and were compared using Pearson's χ^2 test or Fisher's exact test, as appropriate. All tests were two-sided, and $P < 0.05$ was considered statistically significant.

Table 1. Baseline characteristics

Variables	Before matching				After matching			
	Robotic group (*n* = 130)	**Freehand group (*n* = 53)**	***P*-value**	**SMD**	**Robotic group (*n* = 43)**	**Freehand group (*n* = 43)**	***P*-value**	**SMD**
Age	58.29 ± 14.51	61.40 ± 11.59	0.17	0.24	59.79 ± 14.39	61.16 ± 11.33	0.62	0.11
Sex, *n* (%)			0.98	0			0.83	0.05
Male	61 (46.92)	25 (47.17)			19 (44.19)	20 (46.51)		
Female	69 (53.08)	28 (52.83)			24 (55.81)	23 (53.49)		
BMI (kg/m^2)	22.87 ± 3.53	23.06 ± 3.50	0.75	0.05	22.51 ± 3.07	22.89 ± 2.97	0.56	0.13
FEV_1% predicted	86.52 ± 23.27	88.74 ± 25.56	0.6	0.09	88.08 ± 18.28	89.61 ± 25.16	0.75	0.07
Diameter (cm)	1.10 (0.90, 1.67)	1.30 (1.00, 1.90)	0.04	0.29	1.20 (1.00, 1.70)	1.30 (1.00, 1.90)	0.85	0.02
Lobe, *n* (%)			0.43	0.39			0.93	0.15
RUL	37 (28.46)	19 (35.85)			17 (39.53)	16 (37.21)		
RML	12 (9.23)	3 (5.66)			2 (4.65)	3 (6.98)		
RLL	24 (18.46)	7 (13.21)			4 (9.30)	5 (11.63)		
LUL	33 (25.38)	19 (35.85)			15 (34.88)	15 (34.88)		
LLL	24 (18.46)	5 (9.43)			5 (11.63)	4 (9.30)		
Location, *n* (%)			0.74	0.05			0.64	0.1
Periphery	90 (69.23)	38 (71.70)			29 (67.44)	31 (72.09)		
Non-peripheral	40 (30.77)	15 (28.30)			14 (32.56)	12 (27.91)		
Puncture distance (mm)	79.10 ± 19.27	78.42 ± 22.30	0.85	0.03	75.04 ± 19.73	78.78 ± 22.36	0.41	0.18

Puncture distance was not included in the PSM model as it is an intraprocedural variable not available preoperatively; its post-matching SMD (0.18) indicates small residual differences, which were adjusted for in the multivariable logistic regression model. FEV_1: Forced expiratory volume in one second; SMD: standardized mean difference; BMI: body mass index; RUL: right upper lobe; RML: right middle lobe; RLL: right lower lobe; LUL: left upper lobe; LLL: left lower lobe; PSM: propensity score matching.

RESULTS

Baseline characteristics before and after PSM

A total of 183 patients were initially included, comprising 130 patients in the Robotic group and 53 in the Freehand group. Before PSM, baseline characteristics were generally comparable between groups, including age, sex, BMI, FEV_1% predicted, pulmonary lobe distribution, and lesion location (all $P > 0.05$). However, nodules were significantly smaller in the robotic group than in the freehand group (median [IQR], 1.10 [0.90-1.67] cm *vs.* 1.30 [1.00-1.90] cm; $P = 0.04$). Detailed baseline characteristics before matching are provided in Table 1.

Following 1:1 PSM, 43 matched patients remained in each group. Baseline demographic, pulmonary function, and lesion characteristics were broadly comparable between groups, with no significant differences observed in age, sex, BMI, FEV_1% predicted, lesion diameter, pulmonary lobe distribution, or lesion location (all $P > 0.05$). After matching, the SMDs for sex, FEV_1% predicted, lesion diameter, and lesion location were at or below 0.10, whereas residual imbalances were observed for four variables: age, BMI, pulmonary lobe, and puncture distance. To ensure robustness, these four variables were included as covariates in the post-matching multivariable logistic regression for the primary outcome (pneumothorax), providing additional adjustment beyond PSM. Detailed baseline characteristics before and after matching are summarized in Table 1.

Robotic-assisted navigation improves procedural accuracy and safety

We next compared procedural performance and safety outcomes between robotic-assisted and conventional freehand CT-guided MWA of pulmonary nodules. Technical success was achieved in all patients in both groups (100%). Despite similar treatment success rates, the robotic group required fewer CT acquisitions (median [IQR], 2.0 [1.5-2.0] *vs.* 5.0 [5.0-7.0]; $P < 0.01$), achieved greater puncture accuracy, as reflected by a smaller puncture deviation (3.0 [2.0-4.5] mm *vs.* 6.0 [5.0-9.5] mm; $P < 0.01$), and required fewer needle adjustments (2.0 [1.5-2.0] *vs.* 4.0 [3.0-4.0]; $P < 0.01$), as compared with the freehand group. Consistently, a higher proportion of patients in the robotic group required no more than one needle adjustment (25.58% *vs.* 2.33%; $P < 0.01$).

Improved procedural accuracy was accompanied by a more favorable safety profile. The overall complication rate was lower in the robotic group than in the freehand group (46.51% *vs.* 81.40%; $P < 0.01$), driven primarily by reductions in pneumothorax (27.91% *vs.* 69.77%; $P < 0.01$) and chest drain insertion rates (4.65% *vs.* 20.93%; $P = 0.02$). No significant difference was observed in hemorrhage rate between groups (18.60% *vs.* 16.28%; $P = 0.78$). Detailed procedural and safety outcomes are summarized in Table 2 and illustrated in Figure 4.

To determine whether robotic-assisted navigation was independently associated with reduced pneumothorax risk, multivariable logistic regression analysis was performed after adjustment for age, BMI, lesion diameter, pulmonary lobe, and puncture distance. Robotic-assisted puncture remained independently associated with a lower risk of pneumothorax [odds ratio (OR) 0.160, 95%CI: 0.061-0.420, $P < 0.001$] [Supplementary Figure 1]. Together with the consistent findings observed in the unmatched cohort, these results suggest that robotic assistance may provide a protective effect against pneumothorax, potentially by improving trajectory control and reducing repeated puncture-related parenchymal injury. Consistent findings in the unmatched cohort, including procedural efficiency and complication rates, further support the robustness of these results [Supplementary Table 1, Supplementary Figures 2 and 3].

Robotic-assisted navigation provides reproducible benefits across clinical scenarios

Within the robotic-assisted cohort, puncture distance and lesion diameter were not significantly associated with deviation or needle-adjustment frequency (all $P > 0.05$). Upper-lobe lesions had significantly lower deviation than middle/lower-lobe lesions (2.50 mm *vs.* 4.00 mm; $P = 0.029$), whereas adjustment frequency was comparable across lobes ($P = 0.219$). These findings suggest stable robotic performance across lesion depth and size, although lobar anatomy may influence targeting precision. Detailed results are provided in Supplementary Tables 2 and 3.

Subgroup analyses demonstrated that the advantages of robotic-assisted navigation were consistent across all predefined strata. Robotic-assisted puncture was associated with smaller deviation and fewer needle adjustments than freehand puncture in both ≤ 80 mm and > 80 mm puncture-distance strata, in both upper-lobe and middle/lower-lobe lesions, and in both ≤ 1.0 cm and > 1.0 cm nodules (all $P < 0.001$) [Supplementary Table 2]. No significant interaction was detected between treatment group and any subgroup factor (all interaction $P > 0.05$) [Supplementary Table 4], indicating homogeneous treatment effects across strata. The interaction tests were repeated in the propensity score-matched cohort, where all interaction P values again exceeded 0.05, confirming that treatment effects remained homogeneous across the analysis populations [Supplementary Table 5].

Robotic-assisted navigation demonstrates a short learning curve with preserved procedural performance

Learning curve analysis demonstrated a progressive reduction in needle placement time with increasing operator experience [Figure 5]. Needle placement time declined rapidly during the initial cases and

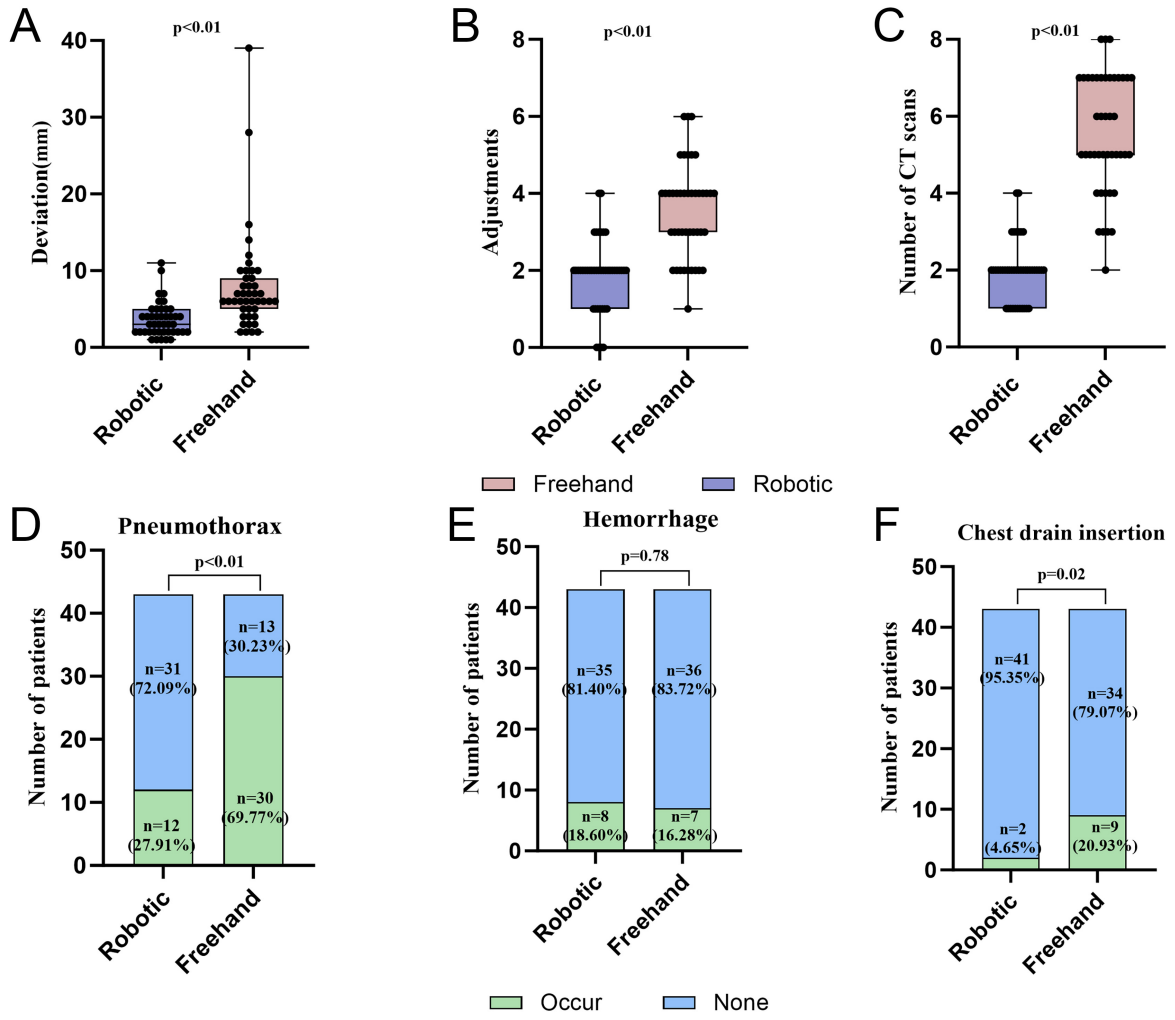


Figure 4. Procedural efficiency and complication incidence after PSM. (A) Puncture deviation; (B) Number of needle adjustments; (C) Number of CT scans; (D) Pneumothorax; (E) Hemorrhage; (F) Chest drain insertion. For (A)-(C), data are presented as median [IQR], and *P* values were calculated using the Mann-Whitney *U* test; scatter plots represent individual values. For (D)-(F), data are presented as incidence rates, and *P* values were calculated using the chi-square test or Fisher's exact test as appropriate; bars display exact numerical proportions within each group. IQR: Interquartile ranges; MWA: microwave ablation; CT: computed tomography.

subsequently approached a plateau. The overall mean needle placement time was 16.97 min. Based on the fitted learning curve, the 50%, 75%, and 90% proficiency milestones were achieved at approximately the 7th, 14th, and 24th procedures, respectively. In this single-operator cohort, needle placement time stabilized after approximately 24 cases, suggesting that the transition from freehand to robotic-assisted technique may have a relatively short learning curve for operators with similar baseline experience.

To further evaluate whether operator experience influenced procedural performance after adoption of robotic navigation, the 130 consecutive robotic-assisted procedures were stratified into a learning phase (first 24 cases) and a proficient phase (subsequent 106 cases). Compared with the learning phase, the proficient phase was associated with a significantly shorter interval from the first CT acquisition to needle placement (16.03 ± 3.08 min *vs.* 21.12 ± 6.56 min; $P < 0.01$) [Table 3]. The number of CT acquisitions and needle adjustments was also significantly reduced in the proficient phase (both $P < 0.01$), reflecting improved procedural efficiency.

Table 2. Outcomes of robotic *vs.* freehand after PSM

Variables	Total (*n* = 86)	Robotic group (*n* = 43)	Freehand group (*n* = 43)	*P*-value
Number of CT scans	3.0 (2.0, 5.0)	2.00 (1.5, 2.0)	5.00 (5.0, 7.0)	< 0.01
Deviation (mm)	5.0 (3.0, 7.0)	3.00 (2.0, 4.5)	6.00 (5.0, 9.5)	< 0.01
Adjustments	2.0 (2.0, 4.0)	2.0 (1.5, 2.0)	4.0 (3.0, 4.0)	< 0.01
Adjustment ≤ 1, *n* (%)				< 0.01
Occur	12 (13.95)	11 (25.58)	1 (2.33)	
None	74 (86.05)	32 (74.42)	42 (97.67)	
Complication, *n* (%)				< 0.01
Occur	55 (63.95)	20 (46.51)	35 (81.40)	
None	31 (36.05)	23 (53.49)	8 (18.60)	
Pneumothorax, *n* (%)				< 0.01
Occur	42 (48.84)	12 (27.91)	30 (69.77)	
None	44 (51.16)	31 (72.09)	13 (30.23)	
Chest drain insertion, *n* (%)				0.02
Occur	11 (12.79)	2 (4.65)	9 (20.93)	
None	75 (87.21)	41 (95.35)	34 (79.07)	
Hemorrhage, *n* (%)				0.78
Occur	15 (17.44)	8 (18.60)	7 (16.28)	
None	71 (82.56)	35 (81.40)	36 (83.72)	

PSM: Propensity score matching; CT: computed tomography.

Notably, puncture accuracy remained stable throughout the learning process, with no significant targeting deviation between the learning and proficient phases (3.0 [2.0-4.0] mm *vs.* 3.0 [2.0-5.0] mm; $P = 0.11$). Similarly, the rates of overall complications, pneumothorax, pulmonary hemorrhage, and chest drain insertion did not differ significantly between phases (all $P > 0.05$). These findings suggest that robotic-assisted navigation may reduce the dependence of procedural quality on operator experience within this single-operator cohort, improving workflow efficiency while maintaining accuracy and safety during early adoption.

DISCUSSION

In this propensity score-matched study, robotic-assisted navigation improved procedural precision, efficiency, and safety during CT-guided percutaneous MWA of pulmonary nodules. The principal findings were threefold. First, robotic-assisted navigation significantly reduced puncture deviation, intraprocedural CT acquisitions, and needle adjustments while maintaining a 100% technical success rate. Second, robotic-assisted puncture was independently associated with a lower risk of pneumothorax, and these benefits were consistently observed across lesions with different sizes, locations, and puncture depths. Third, in this single-operator cohort, procedural efficiency improved rapidly with experience, whereas targeting accuracy and safety remained stable throughout the learning process. Collectively, these findings suggest that the value of robotic-assisted navigation extends beyond technical feasibility and may lie in improving the reproducibility and standardization of CT-guided lung ablation procedures.

Our findings are consistent with previous reports demonstrating the value of robotic assistance in CT-guided lung interventions. Randomized studies of robotic-assisted lung nodule localization have shown improvements in targeting accuracy, first-pass success, procedural efficiency, and radiation exposure without compromising safety[20]. Similarly, robotic-assisted guidance has shown promising accuracy and feasibility in

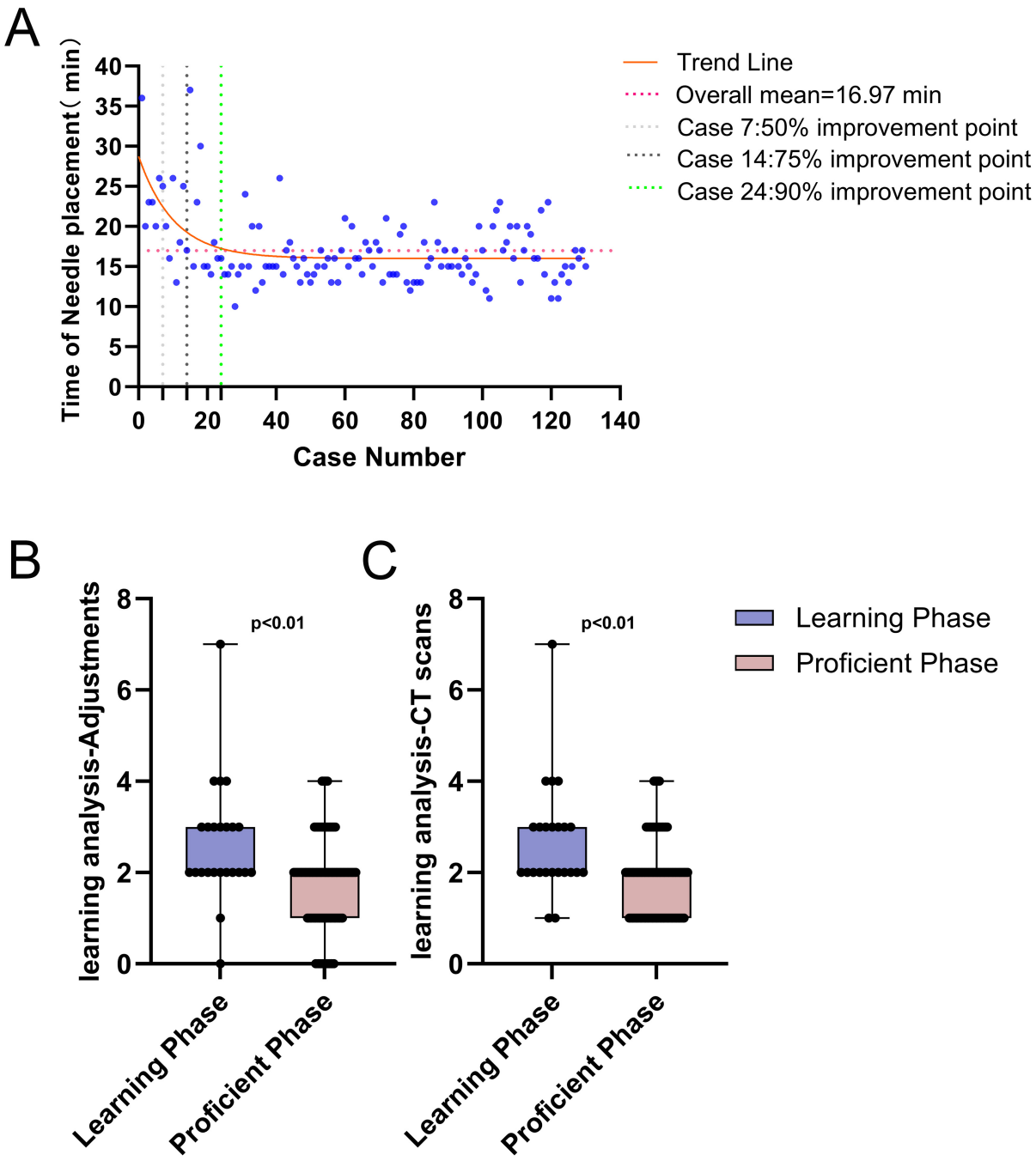


Figure 5. Learning curve of Robotic-Assisted Navigation and analysis. (A) Scatter plot with fitted one-phase exponential decay curve showing the relationship between procedure number and the interval from first CT acquisition to successful needle placement (n = 130 consecutive robotic-assisted procedures). The curve plateau was used to define the learning phase (first 24 cases) and proficient phase (subsequent 106 cases); (B) Box-and-whisker plot of needle adjustment frequency comparing the learning and proficient phases; (C) Box-and-whisker plot of CT acquisition number comparing the learning and proficient phases. For (B) and (C), data are presented as median [IQR], and P values were calculated using the Mann-Whitney U test. IQR: Interquartile ranges; CT: computed tomography.

radiofrequency ablation and cryoablation procedures[21,23]. The present study extends these observations to CT-guided MWA of pulmonary nodules and suggests that the principal advantage of robotic navigation may not be an increase in technical success itself, which is already high in experienced centers, but rather improvements in procedural precision, efficiency, and reproducibility. As image-guided ablation becomes increasingly adopted across institutions with varying levels of expertise, technologies that facilitate standardized procedural execution may become increasingly important.

Table 3. Analysis of procedures and complications in the learning phase *vs.* the proficient phase

Variable	Total (*n* = 130)	Learning Phase (*n* = 24)	Proficient Phase (*n* = 106)	*P* value
Needle placement time (min)	16.97 ± 4.39	21.12 ± 6.56	16.03 ± 3.08	< 0.01
Deviation (mm)	3.0 (2.0, 5.0)	3.00 (2.0, 4.0)	3.00 (2.0, 5.0)	0.11
Adjustments	2.0 (1.0, 2.0)	2.00 (2.0, 3.0)	2.0 (1.0, 2.0)	< 0.01
Number of CT scans	2.0 (1.0, 2.0)	2.0 (2.0, 3.0)	2.00 (1.0, 2.0)	< 0.01
Complication, *n* (%)				0.37
Occur	65 (50.00)	10 (41.67)	55 (51.89)	
None	65 (50.00)	14 (58.33)	51 (48.11)	
Hemorrhage, *n* (%)				0.46
Occur	26 (20.00)	3 (12.50)	23 (21.70)	
None	104 (80.00)	21 (87.50)	83 (78.30)	
Pneumothorax, *n* (%)				0.92
Occur	39 (30.00)	7 (29.17)	32 (30.19)	
None	91 (70.00)	17 (70.83)	74 (69.81)	
Chest drain insertion, *n* (%)				1
Occur	8 (6.15)	1 (4.17)	7 (6.60)	
None	122 (93.85)	23 (95.83)	99 (93.40)	

CT: Computed tomography.

Notably, technical success was achieved in all patients regardless of puncture approach. This finding is unsurprising given the high success rates typically reported for CT-guided lung ablation in experienced centers. Consequently, the clinical value of robotic assistance should not be judged solely by technical success, which may be insufficiently sensitive to detect meaningful procedural improvements. Instead, metrics such as targeting accuracy, needle manipulation, complication rates, and workflow efficiency may better reflect the practical impact of navigation technologies on procedural quality.

The reduction in puncture deviation observed with robotic-assisted navigation may have implications beyond immediate technical performance. In lung ablation, the spatial relationship between the antenna and target lesion directly influences thermal energy distribution and ablative margin formation. Although larger lesions may be relatively tolerant of minor targeting inaccuracies, small deviations may become increasingly important in the treatment of pulmonary nodules, particularly as low-dose CT screening continues to increase detection of sub-centimeter lesions[27,28]. While long-term oncological outcomes were not evaluated in the present study, the improved targeting precision may facilitate more consistent achievement of adequate ablative margins. Whether these technical advantages ultimately translate into superior local tumor control remains an important question for future prospective studies.

A particularly important finding was the substantial reduction in pneumothorax and chest drain insertion associated with robotic-assisted navigation. The magnitude of this benefit appeared greater than would be expected from improved targeting accuracy alone, suggesting that procedural quality in CT-guided lung interventions may depend not only on final needle position but also on trajectory stability and cumulative tissue injury resulting from repeated needle manipulation. In addition to decreasing puncture deviation, robotic-assisted navigation incorporates preprocedural trajectory planning, robotic arm-guided positioning, and respiratory motion monitoring, all of which may contribute to maintaining alignment between the

planned and actual puncture trajectories. By reducing angle deviation, repeated trajectory corrections, and unnecessary needle manipulation, robotic assistance may decrease cumulative pleural and pulmonary parenchymal injury[14,28]. Of note, our pneumothorax ascertainment was highly sensitive, encompassing any imaging-detected pleural air collection regardless of size or clinical significance, including asymptomatic pneumothoraces involving less than 5% lung collapse; the reported rates, particularly in the freehand group, are therefore not directly comparable to studies that report only clinically significant pneumothoraces. From a clinical perspective, reducing pneumothorax and chest drain insertion may be particularly meaningful because these complications can prolong recovery, increase resource utilization, and adversely affect patient experience.

Multivariable and exploratory subgroup analyses further supported the robustness of these findings. After adjustment for age, BMI, lesion diameter, pulmonary lobe, and puncture distance, robotic-assisted puncture remained independently associated with a lower risk of pneumothorax, suggesting that the observed reduction in pneumothorax was unlikely to be solely attributable to differences in baseline characteristics, lesion characteristics, or puncture complexity. Furthermore, the advantages of robotic-assisted navigation in reducing puncture deviation and needle adjustments were consistently observed across lesions with different sizes, locations, and puncture depths, indicating that its benefits are not confined to a specific anatomical scenario but may represent a broader improvement in procedural reproducibility. Nevertheless, within the robotic-assisted cohort, upper-lobe lesions demonstrated slightly smaller puncture deviation than middle/lower-lobe lesions despite comparable adjustment requirements, suggesting that anatomical factors may still influence the ultimate targeting precision. One possible explanation is that upper-lobe lesions are generally less affected by diaphragmatic motion than middle- and lower-lobe lesions, although this hypothesis was not directly evaluated in the present study. Taken together, these findings suggest that robotic-assisted navigation provides stable procedural performance across a broad range of clinical situations while remaining subject to certain anatomical influences.

The reduction in CT acquisitions is also clinically relevant. Although radiation dose was not directly quantified, CT acquisition frequency is widely used as a surrogate for procedural radiation burden in CT-guided interventions[29-31]. Previous studies have reported reductions in radiation exposure with navigation-assisted procedures, particularly when high targeting precision is required[32,33]. The marked decrease in CT acquisitions observed in our study therefore suggests a potential workflow and radiation-related advantage, although dedicated radiation dose metrics will be required to confirm this benefit. Beyond radiation considerations, fewer CT acquisitions may streamline procedural workflow and improve utilization of interventional imaging resources.

The learning-curve analysis provides additional insight into the practical implementation of robotic-assisted navigation[34]. New interventional technologies often improve procedural performance at the expense of increased complexity during early adoption. In contrast, robotic-assisted navigation demonstrated a relatively rapid learning process, with procedural efficiency stabilizing after approximately 24 cases. Importantly, targeting accuracy and complication rates remained stable throughout the learning phase. This finding suggests that increasing operator experience primarily improves workflow efficiency rather than procedural quality. Such observations are consistent with the notion that robotic-assisted navigation may reduce procedural variability by embedding key procedural steps within a standardized platform. From a translational perspective, this characteristic may represent one of the most important advantages of robotic assistance, as it could facilitate broader dissemination of advanced ablation techniques across institutions with different levels of expertise.

Several strengths of this study should be acknowledged. To our knowledge, this is among the largest comparative studies specifically evaluating robotic-assisted navigation for CT-guided percutaneous MWA of pulmonary nodules. In addition to comparing procedural outcomes, we assessed the robustness and implementation characteristics of robotic-assisted navigation through multivariable adjustment, subgroup analyses, and learning-curve evaluation. These complementary analyses provide insight not only into whether robotic navigation is effective, but also into how consistently its benefits are maintained across different clinical scenarios and stages of clinical adoption.

This study also has several limitations. First, this was a retrospective single-center study with a relatively limited matched sample size, and residual confounding cannot be completely excluded despite PSM and multivariable adjustment. Selection bias inherent to the non-randomized design may have influenced treatment assignment, as patients selected the treatment method based on personal preference after physician counseling regarding lesion characteristics and technical feasibility. Although PSM balanced measured baseline covariates, unmeasured confounders may still affect the results. Second, histological confirmation was not available for all nodules. Third, long-term oncological outcomes, radiation dose, and cost-effectiveness were not evaluated. Fourth, no formal a priori power calculation was performed, as this was a retrospective consecutive cohort. Fifth, the complication observation window was limited to the procedure period and the first 24 hours post-procedure; although the majority of procedure-related pneumothoraces occur within this timeframe, rare delayed pneumothoraces and other late complications may therefore have been underestimated[35]. Sixth, multivariable adjustment was performed only for the primary safety outcome (pneumothorax), and secondary outcomes were not formally adjusted for residual covariate imbalance; these findings should therefore be interpreted with appropriate caution. Finally, the learning curve was derived from 130 consecutive procedures performed by a single operator at a single center. Although the operator had extensive prior experience with freehand CT-guided puncture, he had no prior experience with robotic-assisted navigation at the start of the study; therefore, the learning curve reflects the transition from freehand to robotic technique rather than *de novo* acquisition of puncture skills. The approximate 24-case threshold for achieving procedural proficiency may not generalize to operators with different baseline experience levels or to other institutional settings. Additionally, with 42 pneumothorax events and 6 covariates in the multivariable model, the events-per-variable ratio was 7:1; although within the commonly accepted range, the relatively limited sample size may have contributed to wider confidence intervals, which should be considered when interpreting the adjusted estimates. Furthermore, needle placement time was not systematically recorded for the freehand group, precluding a direct comparison of procedural duration between the two puncture techniques.

Nevertheless, improved puncture precision and adequate ablation margins of 5-10 mm may represent favorable technical prerequisites for durable local tumor control, although this hypothesis requires confirmation through standardized follow-up[36,37]. Prospective multicenter studies with long-term follow-up will be necessary to validate the clinical and economic impact of robotic-assisted navigation in CT-guided lung ablation.

Conclusion

Overall, in this propensity score-matched cohort of patients undergoing CT-guided percutaneous MWA of pulmonary nodules, robotic-assisted navigation was associated with improvements in procedural precision, efficiency, and safety, including reduced puncture deviation, fewer CT acquisitions and needle adjustments, and a lower incidence of imaging-detected pneumothorax compared with conventional freehand guidance. The robotic-assisted approach demonstrated consistent procedural performance across the evaluated lesion characteristics and was associated with a relatively short learning curve, supporting its potential as a reproducible and standardized platform for CT-guided pulmonary nodule ablation. Nevertheless, given the

observational, nonrandomized study design and the potential for selection bias related to patient-driven treatment allocation, these findings should be interpreted as associations rather than evidence of causality. Further prospective, multicenter studies are warranted to validate these results and clarify the role of robotic-assisted navigation in CT-guided pulmonary nodule ablation.

DECLARATIONS

Acknowledgments

The authors sincerely thank all patients and their families for their participation in this study. The authors also thank the researchers and clinical staff at the First Affiliated Hospital of Guangzhou Medical University for their contributions to data collection and patient care.

Authors' contributions

Study design, data analysis and interpretation, and manuscript drafting: Li L, Qiu L, Liu H
Data collection and study implementation: Huang L, Cui F, Zhang X, Qu Y
Study conception and design, data analysis and interpretation, manuscript drafting and critical revision, supervision, and funding acquisition: Xue X
Critical revision of the manuscript, supervision, and funding acquisition: Liu J, Liang H
All authors read and approved the final manuscript and agreed to be accountable for all aspects of the work.

Availability of data and materials

For privacy reasons, individual patient data will not be shared publicly. Data generated or analyzed during the study can be requested from the corresponding author.

AI and AI-assisted tools statement

During the preparation of this manuscript, the AI tool ChatGPT (version 5.6, released 2026-07-09) was used solely for language editing. The tool did not influence the study design, data collection, analysis, interpretation, or the scientific content of the work. All authors take full responsibility for the accuracy, integrity, and final content of the manuscript.

Financial support and sponsorship

This study was funded by the Central Government Subsidy Program for Medical Service and Security Capacity Improvement: Public Hospital Comprehensive Reform, 2025, Huizhou Municipal Finance Bureau, China (Hui Cai She [2025] No. 8). The funding body had no role in the design, conduct, analysis, interpretation, or reporting of the study.

Conflicts of interest

All authors declared that there are no conflicts of interest.

Ethical approval and consent to participate

The study was approved by the Institutional Review Board of the First Affiliated Hospital of Guangzhou Medical University (ES-2026-K212-02) on 23 June 2026. As this was a retrospective study, the approval covered the review and analysis of existing clinical data, and the requirement for individual written informed consent for study participation was waived. All patients had provided written informed consent for the procedure at the time of treatment under the hospital's general informed consent for hospitalization.

Consent for publication

Written informed consent for publication of the graphical abstract, which contains an identifiable image of a study team member, was obtained from the individual depicted.

Copyright

© The Author(s) 2026.

Supplementary Materials

Supplementary Materials

REFERENCES

1. Sung H, Filho AM, Laversanne M, et al. Global cancer statistics 2024: GLOBOCAN estimates of incidence and mortality worldwide for 34 cancers in 186 countries. *CA Cancer J Clin.* 2026;76:e70090. DOI PubMed PMC
2. Jonas DE, Reuland DS, Reddy SM, et al. Screening for lung cancer with low-dose computed tomography: updated evidence report and systematic review for the us preventive services task force. *JAMA.* 2021;325:971-87. DOI PubMed
3. Patel P, Pal K, Ahmed H, et al. Using a surgical risk predictor to estimate percutaneous cryoablation adverse event risk: a single center comparative analysis. *J Am Coll Radiol.* 2025;22:550-60. DOI PubMed PMC
4. He JY, Yang L, Wang DD. Efficacy and safety of thermal ablation for patients with stage I non-small cell lung cancer. *Acad Radiol.* 2024;31:5269-79. DOI PubMed
5. Geevarghese R, Alexander ES, Elsakka A, et al. Outcomes following microwave ablation of 669 primary and metastatic lung malignancies. *Eur Radiol.* 2026;36:2295-304. DOI PubMed
6. Zeng C, Lu J, Tian Y, Fu X. Thermal ablation versus wedge resection for stage I non-small cell lung cancer based on the eighth edition of the TNM classification: a population study of the US SEER database. *Front Oncol.* 2020;10:571684. DOI PubMed PMC
7. Lubner MG, Brace CL, Hinshaw JL, Lee FT. Microwave tumor ablation: mechanism of action, clinical results, and devices. *J Vasc Interv Radiol.* 2010;21:S192-203. DOI PubMed PMC
8. Liu J, Jiang Y, He R, et al. Robotic-assisted navigation system for preoperative lung nodule localization: a pilot study. *Transl Lung Cancer Res.* 2023;12:2283-93. DOI PubMed PMC
9. Najafi A, de Baere T, Purenne E, et al. Risk factors for local tumor progression after RFA of pulmonary metastases: a matched case-control study. *Eur Radiol.* 2021;31:5361-9. DOI PubMed
10. Ridouani F, Solomon SB, Bryce Y, Bromberg JF, Sofocleous CT, Deipolyi AR. Predictors of progression-free survival and local tumor control after percutaneous thermal ablation of oligometastatic breast cancer: retrospective study. *J Vasc Interv Radiol.* 2020;31:1201-9. DOI PubMed
11. Kurilova I, Gonzalez-Aguirre A, Beets-Tan RG, et al. Microwave ablation in the management of colorectal cancer pulmonary metastases. *Cardiovasc Intervent Radiol.* 2018;41:1530-44. DOI PubMed PMC
12. Hu Y, Li D, Ding M, et al. Microwave ablation for residual ground-glass nodule-like lung cancer after video-assisted thoracoscopic surgery: a retrospective, large-sample, multicenter study. *Radiol Med.* 2026;131:58-68. DOI PubMed PMC
13. Nakatani M, Kariya S, Ono Y, et al. Radiation exposure and protection in computed tomography fluoroscopy. *Interv Radiol.* 2022;7:49-53. DOI PubMed PMC
14. Huo YR, Chan MV, Habib A, Lui I, Ridley L. Pneumothorax rates in CT-Guided lung biopsies: a comprehensive systematic review and meta-analysis of risk factors. *Br J Radiol.* 2020;93:20190866. DOI PubMed PMC
15. Heerink WJ, Ruiter SJS, Pennings JP, et al. Robotic versus freehand needle positioning in CT-guided ablation of liver tumors: a randomized controlled trial. *Radiology.* 2019;290:826-32. DOI PubMed
16. Schaible J, Pregler B, Verloh N, et al. Improvement of the primary efficacy of microwave ablation of malignant liver tumors by using a robotic navigation system. *Radiol Oncol.* 2020;54:295-300. DOI PubMed PMC
17. Engstrand J, Toporek G, Harbut P, Jonas E, Nilsson H, Freedman J. Stereotactic CT-guided percutaneous microwave ablation of liver tumors with the use of high-frequency jet ventilation: an accuracy and procedural safety study. *Am J Roentgenol.* 2017;208:193-200. DOI PubMed
18. Grössmann-Waniek N, Riegelnegg M, Gassner L, Wild C. Robot-assisted surgery in thoracic and visceral indications: an updated systematic review. *Surg Endosc.* 2024;38:1139-50. DOI PubMed PMC
19. Liu Y, Song Y, Du Y, Qin C, Xu T. From language to world: bridging LLMs and world models for intelligent surgery. *The Innovation Inform.* 2026;2:100040. DOI
20. Deng C, Jiang Y, Lin Y, et al. The effectiveness of robotic-assisted navigation system for preoperative lung nodule localization: a prospective, single-center, non-inferiority, randomized clinical study. *Int J Surg.* 2026;112:7039-50. DOI PubMed
21. Johnston EW, Basso J, Silva F, et al. Robotic versus freehand CT-guided radiofrequency ablation of pulmonary metastases: a comparative cohort study. *Int J Comput Assist Radiol Surg.* 2023;18:1819-28. DOI PubMed PMC
22. Zhang L, Wang L, Kadeer X, et al. ; AME Thoracic Surgery Collaborative Group. Accuracy of a 3-dimensionally printed navigational template for localizing small pulmonary nodules: a noninferiority randomized clinical trial. *JAMA Surg.* 2019;154:295. DOI PubMed PMC
23. Wu X, Wan W, Yang L, et al. Feasibility and safety of a robotic-assisted optical navigation system for pulmonary nodule percutaneous cryoablation: a prospective, single-center, single-arm pilot study. *Respiration.* 2026:1-16. DOI PubMed PMC

24. Song Z, Li Y, Tian Q, et al. Augmented reality guided versus computed tomography guided percutaneous lung nodule localization: a noninferiority randomized clinical trial. *Int J Surg.* 2025;111:2933-41. DOI PubMed PMC
25. Wang J, Yao J, Xu L, et al. Comparison of cyanoacrylate and hookwire for localizing small pulmonary nodules: a propensity-matched cohort study. *Int J Surg.* 2019;71:49-55. DOI PubMed
26. Patel IJ, Rahim S, Davidson JC, et al. Society of interventional radiology consensus guidelines for the periprocedural management of thrombotic and bleeding risk in patients undergoing percutaneous image-guided interventions - Part II: recommendations: endorsed by the Canadian Association for Interventional Radiology and the Cardiovascular and Interventional Radiological Society of Europe. *J Vasc Interv Radiol.* 2019;30:1168-84.e1. DOI PubMed
27. Çakir Ö, Çam I, Koç U, Çiftçi E. Evaluation of major complications associated with percutaneous CT-guided biopsy of lung nodules below 3 cm. *Turk J Med Sci.* 2020;50:369-74. DOI PubMed PMC
28. Ozturk K, Soylu E, Gokalp G, Topal U. Risk factors of pneumothorax and chest tube placement after computed tomography-guided core needle biopsy of lung lesions: a single-centre experience with 822 biopsies. *Pol J Radiol.* 2018;83:e407-14. DOI PubMed PMC
29. Nekolla EA, Brix G, Griebel J. Lung cancer screening with low-dose CT: radiation risk and benefit-risk assessment for different screening scenarios. *Diagnostics.* 2022;12:364. DOI PubMed PMC
30. Leng S, Christner JA, Carlson SK, et al. Radiation dose levels for interventional CT procedures. *AJR Am J Roentgenol.* 2011;197:W97-103. DOI PubMed
31. Betlazar C, Middleton RJ, Banati RB, Liu GJ. The impact of high and low dose ionising radiation on the central nervous system. *Redox Biol.* 2016;9:144-56. DOI PubMed PMC
32. Grasso RF, Luppi G, Cazzato RL, et al. Percutaneous computed tomography-guided lung biopsies: preliminary results using an augmented reality navigation system. *Tumori.* 2018;98:775-82. DOI PubMed
33. Grasso RF, Faiella E, Luppi G, et al. Percutaneous lung biopsy: comparison between an augmented reality CT navigation system and standard CT-guided technique. *Int J Comput Assist Radiol Surg.* 2013;8:837-48. DOI PubMed
34. Guo H, Ouyang Z, Li X, et al. Robotic-assisted CT-guided percutaneous pulmonary nodules localization by hook-wire needles: a retrospective observational study. *J Thorac Dis.* 2024;16:4263-74. DOI PubMed PMC
35. Bae K, Ha JY, Jeon KN. Pneumothorax after CT-guided transthoracic lung biopsy: A comparison between immediate and delayed occurrence. *PLoS One.* 2020;15:e0238107. DOI PubMed PMC
36. Chang ATC, Chan JWY, Siu ICH, et al. Hybrid treatment of multifocal lung malignancy by concomitant transbronchial microwave ablation with same-session lung resection and post-lung resection ablation. *Interdiscip Cardiovasc Thorac Surg.* 2025;40:ivaf152. DOI PubMed PMC
37. Lau KKW, Lau RWH, Baranowski R, Krzykowski J, Ng CSH. Transbronchial microwave ablation of peripheral lung tumors: the NAVABLATE study. *J Bronchology Interv Pulmonol.* 2024;31:165-74. DOI PubMed PMC

Disclaimer/Publisher's Note: All statements, opinions, and data contained in this publication are solely those of the individual author(s) and contributor(s) and do not necessarily reflect those of OAE and/or the editor(s). OAE and/or the editor(s) disclaim any responsibility for harm to persons or property resulting from the use of any ideas, methods, instructions, or products mentioned in the content.

© The Author(s) 2026. Open Access This article is licensed under a Creative Commons Attribution 4.0 International License (https://creativecommons.org/licenses/by/4.0/), which permits unrestricted use, sharing, adaptation, distribution and reproduction in any medium or format, for any purpose, even commercially, as long as you give appropriate credit to the original author(s) and the source, provide a link to the Creative Commons license, and indicate if changes were made.